International Journal of Research in Engineering and Science (IJRES)
ISSN (Online): 2320-9364, ISSN (Print): 2320-9356
www.ijres.org Volume 13 Issue 6 ǁ June 2025 ǁ PP. 21-29

High spatial resolution flaw detector based on the GMR eddy-current probe

Ngoc-Ha Nguyen[1], Thang Nguyen Huu[1*]
[1]*nguyenngocha.osc@gmail.com*
[1*]*nguyenhuuthang@tnut.edu.vn*
[1]*Faculty of Mechanical Engineering, Thai Nguyen University of Technology, Thai Nguyen 250000, Vietnam*

The small feature size and high-sensitivity of the giant magnetoresistance (GMR) sensors make them suitable for miscellaneous applications. In this work, we proposed a novel design of the differential miniature eddy-current probe with a spin-valve GMR sensor. In this differential probe, a full-bridge GMR chip is mounted vertically on the edge of a tiny printed-circuit board to reduce the liftoff distance. The excitation signal is perpendicular to the sensing axis of the GMR chip, which makes it become a differential probe sensitive to the unbalance eddy-current signal on the surface of a conductive sample. The sensor chip is excited by the alternating magnetic field induced by a tiny rectangular coil. The miniature eddy-current probe is sensitive to the surface defect on the flat conductor with a spatial resolution down to 2 mm. The spatial resolution and stability of the device is further verified by taking the two-dimensional scan images over the copper film samples with the surface and subsurface metal losses. The proposed device is useful in the detection of small defects, such as cracks, metal loss, and other mechanical damages.

Index Terms—*Nondestructive testing, Eddy current, Giant magnetoresistance, Defect detection.*

Date of Submission: 24-05-2025 Date of acceptance: 04-06-2025

I. INTRODUCTION

In recent years, the non-destructive inspection (NDI) method based on the eddy-current (EC) effect is increasingly playing an important role in many applications. The advancement in the EC NDI techniques with the miniature magnetic field sensors enables the size estimation of small magnetic particles and the detection of deep-lying defects, such as cracks, metal loss, and other mechanical damages, in highly conductive metals. Several solutions of the field-detection based EC NDI have been developed based on the combination of an excitation coil and magnetic sensors such as Hall [1], giant-magnetoresistance (GMR) [3-5], or superconducting quantum interference device (SQUID) sensors [2]. The high-sensitivity and cost-effect solutions is the technique with GMR sensors, which are suitable for many practical applications, especially on defect evaluation [3]-[5] and magnetic field measurement [6]. Most of the works on the NDI with the magnetoresistive sensors focus on the detection of the surface and subsurface defects. The reliability and capability of GMR sensors for defect detection have been demonstrated by using the eddy-current probe with packaged GMR sensor arrays [4] or a single chip having double-coil excitation [5]. However, the usage of the GMR sensor with a big excitation coil is not suitable for the applications for which the space for scanning the probe is small. Furthermore, the linear arrangement of elements in the array [4]-[8] makes it suitable only to the specimen with a flat surface. Further improvement in the design of the GMR EC probe should be made to enhance the sensitivity and accuracy in flaw characterization. This is especially important in the aerospace industry for the inspection of aircraft structures such as the detection of third-layer cracks at rivet sites [7]-[8]. The spatial resolution of the probe depends on the dimensions of the excitation coil and the sensor size. Namely, reducing the size of the excitation coil or sensor [9],[10] is the only way to enhance the resolution of the probe. The cylindrical coils are frequently used in eddy-current testing due to the fact that it is much easier to compare the results with theoretical analysis. However, it was reported that the pulse-eddy current sensor based on a rectangular coil is advantageous since it fits well to the flat sample surface [11]. By applying the EC imaging technique with a high-resolution probe, the shape of defect can be determined directly without an inversion algorithm for retrieving the geometry of the flaw [12].

In this work, we designed and implemented a miniature eddy-current probe with a GMR sensor. The proposed design aims at enhancing the spatial resolution for detecting the surface and subsurface defects, such as fatigue cracks, inclusions, voids and corrosion for the conductive material or shorts in a printed circuit. The miniature differential EC probe is based on a GMR bare-die sensor and a tiny rectangular exciting coil with a total feature size of less than 3.1 mm. The advantage of the rectangular coil is that its opening fits well to the shape of the GMR sensor. A special aluminum wire bonding technique is used to connect between the terminals of the GMR sensor chip and printed circuit board. The proposed probe is simple in structure and small in size because no auxiliary coil or circuit is needed to compensate the interference induced by excitation. The experimental results on the performance of the proposed probe are analyzed and discussed.

II. EXPERIMENTAL DETAILS

A. Design of the eddy-current probe

The eddy current probe consists of three main parts, including a tiny coil, a GMR sensor and a printed circuit board connecting the terminals of the sensor, as shown in Fig. 1(a). The small excitation coil used in this design is a rectangular copper coil with the geometric parameters as given in

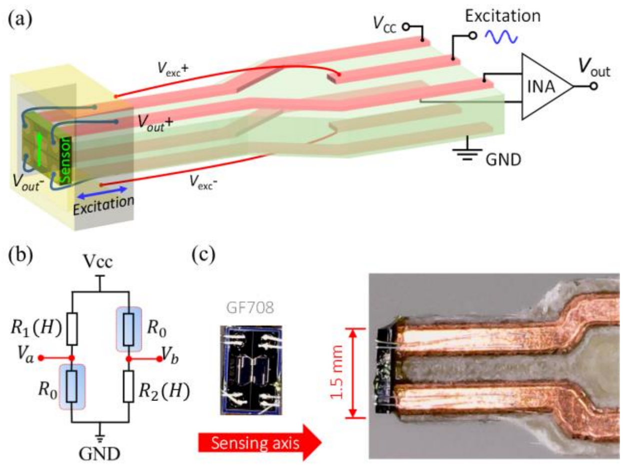

Fig 1. The differential eddy-current probe with a full-bridge GMR sensor chip. (a) The structure of the probe. (b) The equivalent circuit diagram of the GMR chip. (c) Photographs of the GMR chip mounted on the sensor head with the right-angle bonding of aluminum wires.

TABLE I
GEOMETRIC DIMENSIONS OF A RECTANGULAR MODULATION COIL

PARAMETERS	Dimensions
Inside dimensions	1.6 mm × 1.8 mm
Outside dimensions	2.9 mm × 3.1 mm
Length of coil	1.42 mm
Diameter of wire	0.05 mm
Number of turns	252

Table I. The full-bridge GMR sensor used in the probe is from Sensitec GmbH. It consists of two active GMR resistors and two passive resistors. These elements are configured as a Wheatstone bridge circuit on the chip, as shown in Fig. 1(b). The sensitivity of the two active elements, R_1 and R_2, are enhanced by the soft magnetic flux concentrator films, while the two reference elements, R_0, are shielded by the same soft magnetic films to reduce the influence of the applied magnetic field. The sensor output is the potential difference between V_a and V_b:

$$V_{ab} = V_{cc}\left(\frac{R_0}{R_1+R_0}-\frac{R_2}{R_0+R_2}\right) \tag{1}$$

The output depends mainly on the sensing elements of R_1 and R_2. When an external magnetic field (H) is applied along the pinning direction of active elements, the change in the resistance of the of a sensing element can be described by relating the magnetoresistance with the applied magnetic field H as follows [4]:

$$R(H) = R_0\left(1+\frac{r}{r+2}\times\tanh\left(-\frac{H}{H_s}\right)\right) \tag{2}$$

where R_0 is the resistance value at zero magnetic field, H_s is the saturation field, r is the magnetoresistance ratio, and H is the external field. When magnetic field H is the applied on the elements R_1 and R_2, $R_1 = R_2 = R(H)$ in the ideal case. By using the analytic model in (2), the output of the full-bridge sensor becomes:

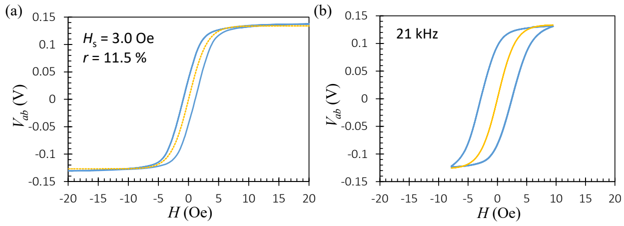

Fig 2. Voltage-field (V-H) curve of the GMR sensor. (a) The *V-H* curve measured at 1 Hz sweeping field. (b) The *V-H* curve at 21 kHz. The orange curves are calculated from (3) with H_s = 3.0 Oe and r = 11.5%.

$$V_{ab} = V_{cc}\left(-\frac{r.\tanh\left(-H/H_s\right)}{2(2+r)+r.\tanh\left(-H/H_s\right)}\right) \qquad (3)$$

The GMR chip is 1 mm in width and 1.4 mm in length, and the sensing axis is along the width of the chip. The measured output characteristics of the GMR sensor at is shown in Fig. 2, where the dotted curve is the plot of (3) with the best fit parameters of H_s = 3.0 Oe and r = 11.5% to the experimental data. This GMR sensor has the linear dynamic range of 0.15 mT with a sensitivity of 91 (mV/V)/mT in a wide range of frequencies (above 1 MHz). To allow the perpendicular excitation field, the GMR chip is attached to the edge of the printed circuit board (PCB) so that the chip surface is perpendicular to the surface of the PCB. This feat is made possible by rotating the PCB to the 90° position during the aluminum wire bonding process, as shown in Fig. 1(a)&(c). This special aluminum wire bonding technique is developed to connect the terminals of the GMR sensor onto both sides of the PCB. With this technique, the distance from the chip surface to the sample surface can be reduced to within 0.2 mm. The sensor surface is perpendicular to the PCB and parallel to the sample surface. The sensing direction of the GMR chip is parallel to the specimen surface and perpendicular to the vertical excitation field. With this arrangement, the GMR chip acts like a gradiometer sensitive to the gradient of the defect field. The miniature chip-and-coil assembly and the short lift-off distance effectively enhance the spatial resolution in flaw detection with the GMR EC probe.

B. Specimens for testing the EC probe

The experiment is conducted on two specimens to determine the spatial resolution in the detection of surface and sub surface flaws. The first sample considered is an aluminum plate with machined simulated cracks for which the depths are

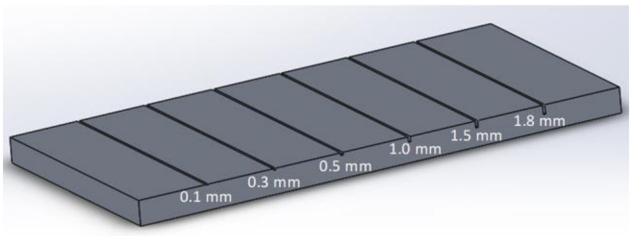

Fig 3. The machined defects on the first sample.

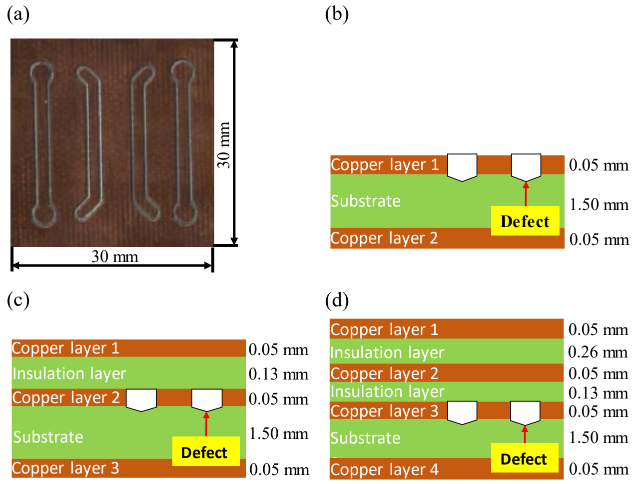

Fig 4. Parameters of the printed circuit board. (a) Photograph of the specimen with machined defects. (b) The structure of 2-layer printed circuit board. (c) The structure of 3-layer printed circuit board. (d) The structure of 4-layer printed circuit board.

0.1, 0.3, 0.5, 1.0, 1.5 and 1.8 mm and the widths are 0.2 mm, as shown in Fig 3. The inter-crack distance is 14.3 mm. The length, width and height of the plate are 100, 50 and 5 mm respectively.

The second type of sample is the multi-layer printed circuit board, which is designed to investigate the ability of the EC probe to detect the defects in the top and underlying layers at different depths on the PCB. These samples are 30 mm×30 mm in dimension with 2, 3, or 4 layers of copper films, as shown in Fig. 4. The simulated hidden defects, which are slots of 0.8 mm width cut by an engraving machine, are on the top, second, and third copper layer, respectively. The multi-layer structure is formed by attaching the copper films of 50-μm thickness bonded with the insulation layers of 0.13 mm and 0.26 mm thicknesses. The liftoff distances from the bottom of the probe to the position of the defect are 0.2, 0.38, 0.69 mm respectively for the 2-layer, 3-layer, and 4-layer PCB samples.

C. Computer-Controlled Measurement System

The computer-controlled measurement system for testing the performance of the GMR EC sensor is shown in Fig. 5. To test the spatial resolution in the detection of defects, the sample was placed on the translation stage controlled by the 08TMC-2 motor controller from Unice E-O Services Inc. The spatial resolution for the scanning motion is 1.25 μm. In order to scan for the simulated defect in the sample and to avoid interference induced by bending the signal transmission wires during scanning, the EC probe is static while the object under test is moving. The GMR EC probe is driven by a sine wave voltage provided by a function generator of controlled amplitude (up to 10 V) and frequency (above 1 MHz). The differential output of the probe is measured by a low noise preamplifier and transmitted to the lock-in amplifier to analyze the amplitude and phase of the EC signal. The spatial distribution of the signals was digitized in real time by a data acquisition (DAQ) module USB-6216 from National Instruments and recorded by the computer with the sampling rate of 400 kS/s. An in-house developed C# program is used to set the scanning range, velocity, and step size as well as to record the demodulated EC signal taken by the DAQ device. When not specified, the excitation voltage used in this experiment is 2.1 V in peak-to-peak amplitude, while the DC bias voltage for driving the GMR sensor is 4.65 V in all of the experiments.

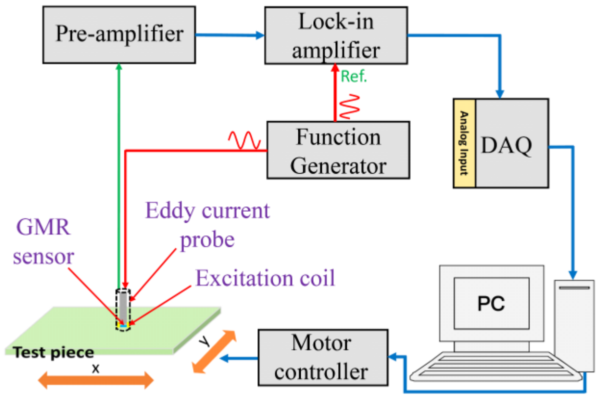

Fig 5. The function block diagram of the eddy-current automatic inspection system.

III. RESULTS AND DISCUSSION

D. Crack inspection for the aluminum plate

First, the experiment is performed on the aluminum plate with machined slots, as shown in Fig. 3. The sensing axis of the GMR sensor is perpendicular to the direction of the simulated cracks in this case. When the aluminum plate moves under the probe along the sensing axis of the GMR sensor, the in-phase (V_i) and quadrature (V_q) eddy-current signals are recorded and analyzed to investigate their dependence on the position and depth of the defect. In order to find out the optimal parameter for flaw detection, the EC signal at various excitation frequencies were tested on the same specimen.

Fig. 6 depicts the 1D signal scan result with the GMR EC probe over a surface crack of 1.5 mm depth at the excitation frequencies of 5, 10, 17, 21, 25 and 30 kHz. The obtained waveforms are generally antisymmetric to the center of the crack when the baseline voltage at the corresponding frequency is subtracted. The remaining drift in the baseline voltage may be attributed to imbalance in the coil construction as well as in the probe assembly, which results in the frequency-dependent output affected by the skin effect and capacitive coupling in the coil. To estimate the output amplitude, the EC signal is integrated over the coordinate of the position by using the following relations:

$$\text{Int. Amp} = \sqrt{\left(\int_0^x V_i dx\right)^2 + \left(\int_0^x V_q dx\right)^2} \quad (4)$$

$$\text{Int. Phase} = \text{atan2}\left(\int_0^x V_i dx, \int_0^x V_q dx\right) \quad (5)$$

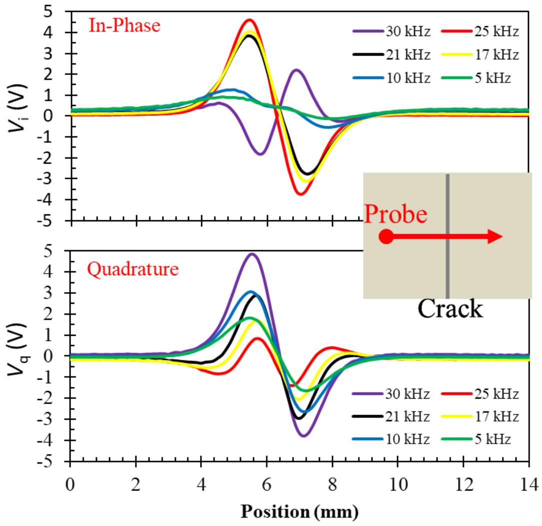

Fig. 6. In-phase and quadrature components of the output voltage near a 1.5 mm deep crack under various excitation frequencies.

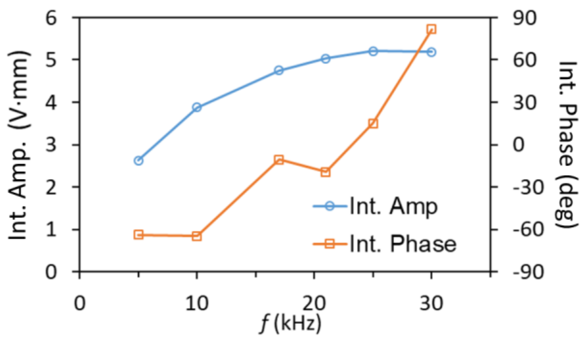

Fig. 7. The integrated amplitude and phase of the EC signals at the position of the 1.5-mm crack under various excitation frequencies.

where x is the coordinate of position in Fig. 6, and atan2 is the two-argument arctangent function. It was found that the output amplitude increases with the excitation frequency until 30 kHz, above which the signal amplitude does not increase significantly, as shown in Fig. 7. The phase of the integrated signal changes rapidly at frequencies close to 30 kHz, indicating that the saturation in the integrated amplitude is owing to the bandwidth limit of the excitation coil.

The one-dimensional (B-scan) curve over the aluminum plate with simulated cracks of depth ranging from 0.1 to 1.8 mm is shown in Fig. 8. The lift-off distance between the probe and the specimen is 0.2 mm, and the excitation frequency is 30 kHz. It was found that all of the cracks on the aluminum plate are detected by the EC probe, and the maximum change in the in-phase and quadrature output voltages occurs right at the position of cracks. As the baseline voltage fluctuates over the scanning range, the Gaussian spatial filter [13] is applied to generate the distribution of the approximate baseline voltage and subtract from V_{out} before integration. In this way, the integrated amplitude obtained is roughly proportional to the crack depth, as shown in Fig. 8(b). The full width at half maximum of each peak near the crack is less than 2 mm, which has achieved the physical limit set by the lateral size of probe. The amplitude and phase plots in

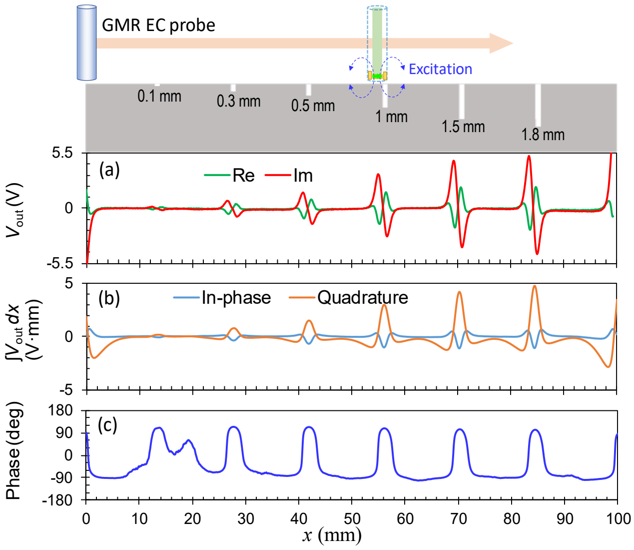

Fig. 8. The integrated in-phase (Re) and quadrature (Im) signals for the output voltage of EC probe when scanning on the aluminum plate at the excitation frequency of 30 kHz.

Fig. 8(b) and (c) indicate that all of the surface cracks deeper than 0.1 mm can be identified clearly with the proposed GMR EC probe.

E. Defect inspection on multi-layer printed circuit board

To test the performance of the EC probe in imaging the geometry of two-dimensional (2D) defects, a printed circuit board with the machined defects depicted in Fig. 4(a) is used as specimen in the 2D imaging (C-scan) experiment. To detect the defects in the underlying layer, it is necessary to lower the frequency of the excitation coil to increase the penetration depth. After taking the C-scans for multiple excitation frequencies, it was found the that the best sensitivity for the deeper flaw is achieved at the excitation frequency of 21 kHz. The skin depth of the eddy-current at this excitation frequency is 0.45 mm, which is more than the total thickness of 0.2 mm for the copper layers. To take the 2D image, the specimen is moved with the step size of 0.0625 mm relative to the static probe. The in-phase and quadrature voltages were recorded to form the image of the defect signal over the surface of the specimen.

Fig. 9, 10 and 11 show the amplitude and phase maps of the defect signal for the 2-layer, 3-layer, 4-layer PCB samples with the defect layer at the depth of 0, 0.18 and 0.49 mm, respectively. It can be seen that the geometry of the defect can be identified clearly from the amplitude and phase images for the depth 0 mm. The defect features in the amplitude image are significantly smoothed out with the increasing depth, while the defect profile remains clear in the phase image up to 0.49 mm. The amplitude and phase values are affected by the number of top cooper layers. Specifically, the range of the amplitude and phase values is gradually decreased. The minimum and maximum values are extracted from the line at $y = 15$ mm perpendicular to the slot axes. For the 2-layer, 3-layer, and 4-layer PCBs, the difference between the peak and valley of amplitude are 3.3 V, 1.1 V, and 1.0 V, while the difference between the peak and valley of phase are 32°, 24°, and 13°, respectively. Since the change in amplitude is more significant, it can be seen that the response of the amplitude values is disturbed when the liftoff distance of the probe increases. For 4-layer printed circuit board with the liftoff distance of 0.69 mm, the amplitude image was significantly blurred while the response of the phase values is slightly changed and the phase images still clearly reveal the defects on PCB samples. Fig. 12 shows that the full width at half maximum of each peak near slot positions of the crack is less than 2 mm, which has achieved the physical limit set by the lateral size of the probe.

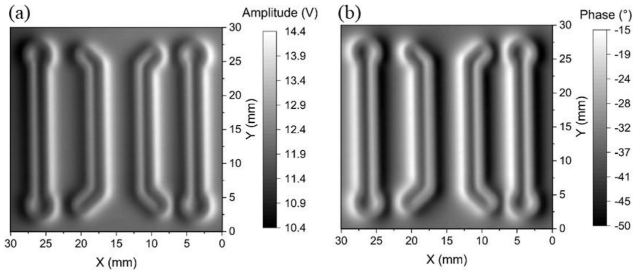

Fig 9. C-scan image for 2 layer printed circuit board: (a) the amplitude image, (b) the phase image.

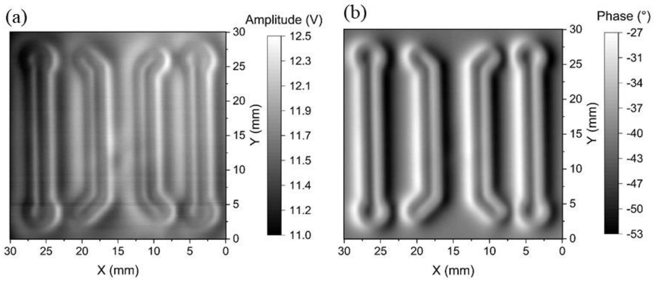

Fig 10. C-scan image for 3 layer printed circuit board: (a) the amplitude image, (b) the phase image.

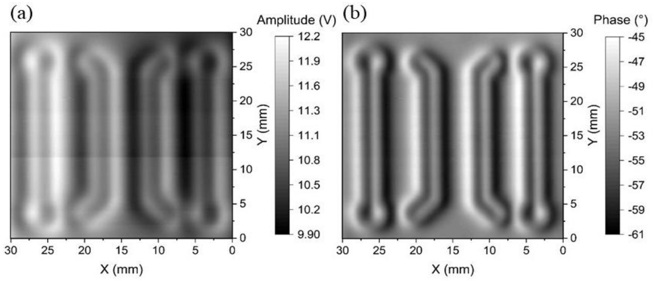

Fig 11. C-scan image for 4 layer printed circuit board: (a) the amplitude image, (b) the phase image.

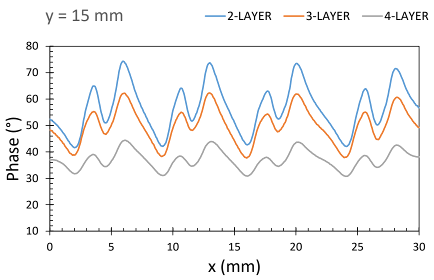

Fig 12. The phase signal is extracted from the line at y = 15 mm .

The result indicates that the developed GMR EC probe is useful in the characterization of surface and subsurface defects in the multilayer printed circuit board.

IV. CONCLUSION

The novel design of the proposed eddy-current probe based on the GMR sensor can achieve high spatial resolution and high sensitivity. It is capable of detecting the metal loss with a feature size less than 1 mm in the conductive objects. The experimental results show that the surface flaw with a minimum depth of 0.1 mm can be detected on the aluminum sample. The 2D eddy-current image taken by using the developed probe can locate the position of defects and evaluate their geometric features on the PCB sample with the hidden defect covered by two layers of 50-μm copper films. In addition, due to the tiny size of GMR sensor, the probe can map the distribution of the secondary magnetic field induced by the eddy current, which is valuable for the inverse calculation to determine the local electromagnetic properties of the conductive specimens.

ACKNOWLEDGMENT

This work is supported by the Ministry of Science and Technology of Taiwan under Grant No. MOST108-2221-E992-083MY2.

REFERENCES

[1]. A. L. Ribeiro, H. G. Ramos, "Inductive Probe for Flaw Detection innon-Magnetic Metallic Plates Using Eddy Currents", IEEE Instr. &Meas. Tech. Conf., I2MTC, Victoria, Canada, pp. 1447-1451, 2008.
[2]. W. G. Jenks, S. S. H. Sadeghi, and J. P. Wikswo, Jr, "SQUIDS for nondestructive evaluation," J. Phys. D: Appl. Phys., vol. 30, pp. 293–323,1997.
[3]. D. Rifai, A. N. Abdalla, K. Ali, & R. Razali, "Giant magnetoresistance sensors: A review on structures and non-destructive eddy current testing applications", Sensors, 16(3), 298 (2016).
[4]. O. Postolache, A. L. Ribeiro, and H. G. Ramos, "GMR array uniform eddy current probe for defect detection in conductive specimens", Measurement, 46(10), 4369-4378 (2013).
[5]. Andrea Bernieri, Luigi Ferrigno, Marco Laracca, and Antonio Rasile, "Eddy Current Testing Probe Based on Double-Coil Excitation and GMR Sensor", IEEE Transactions on Instrumentation and measurement, vol. 68, no. 5, pp. 1533 – 1542(2019).
[6]. V. S. Luong, Y.-H. Su, C.-C. Lu, J.-T. Jeng, J.-H. Hsu, M.-H. Liao, J.-C. Wu, M.-H. Lai, C.-R. Chang, "Planarization, Fabrication and Characterization of Three-dimensional Magnetic Field Sensors", IEEE Transactions on Nanotechnology, Vol. 17, no. 1, pp.11 - 25 (2018).
[7]. J. Kim, G. Yang, L. Udpa, & S. Udpa, "Classification of pulsed eddy current GMR data on aircraft structures", Ndt & E International, 43(2), 141-144 (2010).
[8]. C. H. Smith, R. W. Schneider, T. Dogaru, & S. T. Smith, "Eddy-Current Testing with GMR Magnetic Sensor Arrays", In AIP Conference Proceedings, Vol. 700, No. 1, pp. 406-413, American Institute of Physics (2004, February).
[9]. T. Dogaru and S. T. Smith, "Giant magnetoresistance-based eddy-current sensor", IEEE Transactions on Magnetics, 37(5), 3831-3838 (2001).
[10]. D. Pasadas, T. Rocha, H.G. Ramos, A.L. Ribeiro, "Evaluation of portable ECT instruments with positioning capability", Measurement, 45 (1) (2012), pp. 393-404.
[11]. Y.Z. He, F.L. Luo, M.C. Pan, X.C. Hu, J.Z. Gao, B. Liu, "Defect classification based on rectangular pulsed eddy current sensor in different directions", Sens. Actuators A 157 (2010) 26–31.
[12]. Y. He, F. Luo, and M. Pan, "Defect characterisation based on pulsed eddy current imaging technique," Sensors Actuat. A: Phys., vol. 164, pp. 1–7, Sep. 2010.
[13]. P. Getreuer, "A survey of Gaussian convolution algorithms", Image Processing On Line, 2013, 286-310 (2013).